Original Article

MOLECULAR METABOLISM

CX3CL1-Fc treatment prevents atherosclerosis in *Ldlr* KO mice

Matthew Riopel [1], Melanie Vassallo [2], Erik Ehinger [2], Jennifer Pattison [1], Karen Bowden [1], Holger Winkels [2], Maria Wilson [3], Ron de Jong [3], Sanjay Patel [3], Deepika Balakrishna [3], James Bilakovics [3], Andrea Fanjul [3], Artur Plonowski [3], Christopher J. Larson [3], Klaus Ley [2], Pedro Cabrales [4], Joseph L. Witztum [1], Jerrold M. Olefsky [1,], Yun Sok Lee [1,*]**

ABSTRACT

Objective: Atherosclerosis is a major cause of cardiovascular disease. Monocyte-endothelial cell interactions are partly mediated by expression of monocyte CX3CR1 and endothelial cell fractalkine (CX3CL1). Interrupting the interaction between this ligand—receptor pair should reduce monocyte binding to the endothelial wall and reduce atherosclerosis. We sought to reduce atherosclerosis by preventing monocyte-endothelial cell interactions through use of a long-acting CX3CR1 agonist.

Methods: In this study, the chemokine domain of CX3CL1 was fused to the mouse Fc region to generate a long-acting soluble form of CX3CL1 suitable for chronic studies. CX3CL1-Fc or saline was injected twice a week (30 mg/kg) for 4 months into Ldlr knockout (KO) mice on an atherogenic western diet.

Results: CX3CL1-Fc-treated *Ldlr* KO mice showed decreased en face aortic lesion surface area and reduced aortic root lesion size with decreased necrotic core area. Flow cytometry analyses of CX3CL1-Fc-treated aortic wall cell digests revealed a decrease in M1-like polarized macrophages and T cells. Moreover, CX3CL1-Fc administration reduced diet-induced atherosclerosis after switching from an atherogenic to a normal chow diet. In vitro monocyte adhesion studies revealed that CX3CL1-Fc treatment caused fewer monocytes to adhere to a human umbilical vein endothelial cell monolayer. Furthermore, a dorsal window chamber model demonstrated that CX3CL1-Fc treatment decreased in vivo leukocyte adhesion and rolling in live capillaries after short-term ischemia-reperfusion.

Conclusion: These results indicate that CX3CL1-Fc can inhibit monocyte/endothelial cell adhesion as well as reduce atherosclerosis.

Keywords Fractalkine; CX3CR1; Atherosclerosis; Monocyte adhesion; Inflammation; *Ldlr* KO

1. INTRODUCTION

Cardiovascular disease (CVD) accounted for an estimated 31.5% of global deaths in 2013 [1]. While all the multifactorial mechanisms underlying atherosclerosis are not fully known, strong associations with hypercholesterolemia [2], obesity [3], type 2 diabetes (T2DM) [4], and insulin resistance [5] have been shown.

The development of atherosclerotic plaques involves enhanced LDL trapping in the intima and formation of oxidized LDL, which leads to a series of processes including adhesion of monocytes to the endothelium, macrophage infiltration, cytokine release, and foam cell formation [6]. Thus, macrophage accumulation during atherosclerosis progression contributes to inflammatory gene expression, foam cell accumulation, smooth muscle cell modulation, and endothelial wall thickening [7]. Recruitment of monocytes to the endothelium is a key step in the development of atherosclerosis, and targeting this step can inhibit lesion formation [8]. Two primary monocyte subsets exist in mice, classical Lys6C^{hi}CX3CR1^{lo} and patrolling Lys6C^{lo}CX3CR1^{hi} cells. Both monocyte subsets are recruited to atherosclerotic vessels, but the majority are Lys6C^{hi} [9]. Once in the inflamed vessel, these monocytes can differentiate to M1-like macrophages that take up lipid and become foam cells [10]. Endothelial cells also play a critical role in atherosclerosis, whereby pro-inflammatory conditions (e.g. high fat/high cholesterol diet) promote leukocyte adhesion [11].

Fractalkine (CX3CL1) and its cognate receptor CX3CR1 are important for immune cell trafficking [12]. CX3CL1 is expressed as a membrane-bound protein (mCX3CL1), and the extracellular domain can be cleaved and released into the circulation for actions at distal sites [13]. During atherosclerosis, blood monocytes expressing CX3CR1 bind to blood vessel endothelial cells-expressing mCX3CL1, promoting monocyte adhesion [14]. The clustering of CX3CR1 receptors on the cell surface further promotes adhesiveness between monocytes and endothelial cells [15]. Several studies demonstrate that genetic deletion of either CX3CL1 or CX3CR1 protects mice against atherosclerosis [16—18]. In

[1]Division of Endocrinology & Metabolism, Department of Medicine, University of California, San Diego, La Jolla, CA, USA [2]Division of Inflammation Biology, La Jolla Institute for Allergy and Immunology, La Jolla, CA, USA [3]Cardiovascular and Metabolic Diseases Drug Discovery Unit, Takeda Pharmaceuticals, San Diego, CA, USA [4]Department of Bioengineering, University of California, San Diego, La Jolla, CA, USA

*Corresponding author. Stein Clinical Research Building, Room 231, 9500 Gilman Drive, MC# 0673, La Jolla, CA, 92093, USA. E-mail: yunsoklee@ucsd.edu (Y.S. Lee).

**Corresponding author. Stein Clinical Research Building, Room 227, 9500 Gilman Drive, La Jolla, CA, 92093, USA. E-mail: jolefsky@ucsd.edu (J.M. Olefsky).

Received June 15, 2018 • Revision received November 16, 2018 • Accepted November 29, 2018 • Available online 2 December 2018

https://doi.org/10.1016/j.molmet.2018.11.011

Abbreviations

CVD	Cardiovascular disease
DWCM	Dorsal window chamber model
FCD	Functional capillary density
CX3CL1	Fractalkine
CX3CL1-Fc	Fractalkine Fc fusion protein
HCD	High cholesterol (1%)/low fat (4.4%) diet
Hct	Hematocrit
HUVEC	Human umbilical vein endothelial cells
HR	Heart rate
i.p.	Intraperitoneal
KO	Knockout
LDL	Low-density lipoprotein
LDLR	Low-density lipoprotein receptor
MAP	Mean arterial blood pressure
mCX3CL1	Membrane-bound fractalkine
NCD	Normal chow diet
T2DM	Type 2 Diabetes Mellitus
VEH	Vehicle or saline treatment
WD	Western diet

addition, subjects carrying a loss of function CX3CR1 M280 variant show protection against atherosclerosis [19]. Collectively, these studies suggest that interfering with monocyte CX3CR1 and endothelial cell mCX3CL1 may be protective against atherosclerosis.

On the other hand, CX3CR1 KO mice demonstrate exaggerated hepatic inflammation and fibrosis when they are experimentally induced through CCl_4 administration or bile duct ligation [20,21]. Moreover, CX3CR1 KO mice exhibit impaired glucose tolerance with decreased beta cell insulin secretion, whereas administration of a long acting CX3CL1, tethered to the mouse Fc fragment (CX3CL1-Fc), improved insulin secretion, insulin sensitivity, and glucose tolerance [22]. These results indicate that soluble CX3CL1 administration exerts beneficial effects on metabolic health. However, since genetic loss of CX3CR1 or CX3CL1 is atheroprotective, one could raise a safety concern that a soluble CX3CL1-Fc agonist might promote atherosclerosis.

In the current studies, we propose the opposite, hypothesizing that soluble CX3CL1-Fc can act as an agonist against CX3CR1, disrupting the interaction between monocytes and endothelial cells mediated by endogenous mCX3CL1 and CX3CR1. To address this hypothesis, we adopted in vitro and in vivo model systems that assess monocyte-endothelial cell interactions in stressed conditions. We also tested the effect of chronic CX3CL1-Fc administration on atherosclerosis prevention, treatment, and after diet switch. We find that CX3CL1-Fc decreases monocyte adhesion to the endothelium both in vitro and in vivo. Moreover, we also demonstrate that CX3CL1-Fc treatment reduced atherosclerosis throughout the aorta and aortic root in hypercholesterolemic *Ldlr* KO mice without changes in plasma cholesterol levels. These beneficial changes were associated with reduced aortic M1-like macrophages and T cells.

2. MATERIAL AND METHODS

2.1. Experimental mouse model

Eight week-old male C57BL/6 WT and ten week-old male *Ldlr* KO mice on the C57BL/6 background were obtained from Jackson Labs (catalog# 002207). CX3CL1-Fc was produced in collaboration with Takeda California, Inc.

a) *Prevention Study*: *Ldlr* KO mice were fed either a high cholesterol (1%)/low fat (4.4%) diet (Envigo, catalog# TD.97131) or a high cholesterol (1.25%)/high fat (40%) WD (Envigo, catalog# TD.02028) and randomized to be injected with either CX3CL1-Fc (30 mg/kg) or saline (VEH) intraperitoneally twice a week for 4 months. This dosing regimen is slightly modified from our previous studies demonstrating the anti-diabetic effects of CX3CL1-Fc [13].
b) *Treatment Study*: *Ldlr* KO mice were fed a high cholesterol/high fat diet (Research Diets, catalog# D12108C) for 8 months. At 4 months, a group of mice were sacrificed for baseline measurements and the remaining were randomly split into two groups, one injected intraperitoneally with CX3CL1-Fc (30 mg/kg) and the other with saline (VEH) twice a week for the remaining 4 months.
c) *Reversion Study*: *Ldlr* KO mice were fed a high cholesterol/high fat diet (Research Diets, catalog# D12108C) for 4 months and a group of mice were sacrificed for baseline measurements. The remaining mice were switched to a normal chow diet (NCD) and split into two groups, one injected intraperitoneally with CX3CL1-Fc (30 mg/kg) and the other with saline (VEH) twice a week and were sacrificed at 4 and 8 months after treatment began.

Mouse tissues collected and processed as detailed below.

2.2. Flow cytometry

a) *Endotheliums*: Aortas/carotids were collected from *Ldlr* KO mice after their respective treatment regimen. Following euthanasia and heparin perfusion, tissues were cut up and placed in a tube containing a digestion cocktail of 450 U/mL Collagenase I, 250 UmL Collagenase XI, 120 U/mL Hyaluronidase, and 120 U/mL DNase I. These tubes were placed in a shaking incubator at 150 rpm and 37 °C for 60 min. Following digestion, the digestion cocktail was passed through a 70 μm filter into a fresh 15 ml conical tube, and then centrifuged at 500 g and 4 °C for 5 min.
b) *Other Tissues*: Spleens, blood, bone marrow, cervical lymph nodes, axillary lymph nodes, mesenteric lymph nodes, and paraaortic lymph nodes were collected from *Ldlr* KO mice after their respective treatment regimen. After euthanasia and heparin perfusion, spleens and lymph nodes were pushed through 70 μm filters into conical tubes, and filters were washed with PBS. Tubes were centrifuged for 5 min at 4 °C and 500 g.

After aspirating supernatant and resuspending pellets, cells were incubated with Zombie Red Viability Dye (Biolegend, catalog# 423110) for 30 min at 4 °C, then washed. Single cell suspensions were then incubated with mouse FcR blocking reagent (Miltenyi Biotec, catalog# 130-092-575), and the following extracellular antibodies for 30 min at 4 °C: AlexaFluor700-conjugated anti-CD45 (Biolegend, catalog# 103128), APC-eFluor780-conjugated anti-TCR-β (eBioscience, catalog# 47-5961-82) or PerCP-Cy5.5-conjugated anti-CD3 (Biolegend, catalog# 100218), PerCP-conjugated anti-CD4 (Biolegend, catalog# 100538), BV421-conjugated anti-CX3CR1 (Biolegend, catalog# 149023), PE-Cy7-conjugated anti-CD69 (Biolegend, catalog# 104512), APC-conjugated anti-CD103 (Biolegend, catalog# 121414), BV711-conjugated anti-CD11b (Biolegend, catalog# 101242), FITC-conjugated anti-CD64 (Biolegend, catalog# 139316), BV605-conjugated anti-CD8a (Biolegend, catalog# 100744), BV510-conjugated anti-CD86 (Biolegend, catalog# 105040), and PE-conjugated anti-CD206 (Biolegend, catalog# 141706). Following incubation, cells were washed, and then fixed according to the eBioscience fixation buffer protocol. Data were acquired on the BD LSRII

cytometer using FACSDiva software, and raw data were analyzed using FlowJo software.

For analysis of monocyte development, single cell suspensions of bone marrow or spleen were stained with live/dead fixable aqua cell stain kit (ThermoFisher, catalog# L34957) and then the following antibodies: APC-conjugated anti-Gr-1 (Biolegend, catalog# 108411), PerCP5.5-conjugated CD45 (Biolegend, catalog# 103131), PE-conjugated Ly-6C (Biolegend, catalog# 128007), FITC-conjugated CD11b (Biolegend, catalog# 101205) and PE/Cy7-conjugated F4/80 (Biolegend, catalog# 123113). Following incubation, cells were washed, and then fixed according to the eBioscience fixation buffer protocol. Data were acquired on the BD Canto (RUO Orange) and then analyzed using Flowjo software.

2.3. En face and aortic root analyses

At specified time points, *Ldlr* KO mice on their respective diet regimen and treated ± CX3CL1-Fc were euthanized by a lethal dose of pentobarbital, and the circulation was perfused with isotonic EDTA-PBS solution. This was followed by in situ fixation at physiological pressure with formal sucrose (4% paraformaldehyde). Aortas were then dissected, opened longitudinally, thoroughly cleansed of adventitial tissue, and stained with Sudan IV, as previously described [23]. Aortas were pinned out on a black wax pan (after adventitial removal), and the percentage of atherosclerotic surface area was determined by computer-assisted image analysis, as previously described in detail [23].

At sacrifice, the heart and proximal aorta were obtained, embedded in Optimal Cutting Temperature compound, and stored at −70 °C. Aortic root cross-sectional atherosclerosis was measured by cutting 10 μm paraffin sections from the site where the first leaflet was seen until the last leaflet. Sections at every 100 μm interval from the first leaflet were stained with Oil Red O and hematoxylin. Quantitative analysis of lesion and necrotic area was performed on each section with about 7—10 sections analyzed, spanning 1000 μm from the origin of the first visible leaflet. The results are presented as total lesion or necrotic area in mm^2 of all aortic cross sections analyzed [24].

2.4. Plasma cholesterol/triglyceride assays and lipoprotein profiling

Plasma cholesterol was measured using a Cobas AutoAnalyzer with a Cholesterol CHOD-PAP kit as per the manufacturer's instructions (Roche, catalog# 11,491,458-216). Plasma triglycerides were measured with a Triglyceride —SL kit from Sekisui Diagnostics as per their instructions (catalog# 236-60). Cholesterol and triglyceride lipoprotein profiling was performed using fast performance liquid chromatography (FPLC) with a Superose 6 column as described previously [24].

2.5. Monocyte adhesion assays

a) *Static*. C57/BL6 male mouse peripheral blood monocytes were isolated as per the manufacturer's instructions (EasySep Mouse Monocyte Isolation Kit, STEMCELL Technologies, catalog# 19861). Monocytes or human THP-1 cells (ATCC, catalog# TIB-202) were stained green with PKH67 (Sigma, catalog# PKH67GL-1 KT, St. Louis, MO, USA), pre-incubated in CX3CL1-Fc (1.4 nmol/L) or saline (VEH)-containing medium for 30 min and then added to washed human umbilical vein endothelial cell (HUVECs) (ATCC, catalog# PCS-100-010) monolayers for 1 h. For LPS stimulation (Sigma, catalog# LPS25), HUVEC monolayers were pre-treated with 100 ng/ml LPS for 30 min, while monocytes or human THP-1 cells were pre-treated with CX3CL1-Fc (1.4 nmol/L) or saline for 30 min before layering on confluent LPS-stimulated HUVECs. After 1 h incubation, PFA fixation, washing, DAPI staining and slide mounting occurred. An Olympus FV1000 Confocal Microscope was used to collect images of monocytes or THP-1 cells bound to endothelial cells. Data are presented as % PKH67+ cells over number of endothelial cells.

b) *Flow*. THP-1 monocytes were labeled with PKH67 (Sigma) then pre-incubated with CX3CL1-Fc (1.4 nmol/L) or saline (VEH) for 30 min. Collagen I-coated glass slides plated with HUVECs until 100% confluency were washed with RPMI 1640 and then assembled into flow chambers and connected to a parallel flow system for analyses [25]. The HUVEC monolayer was exposed to a steady shear stress of 1 dyne/cm^2 of treated THP-1 cells for 10 min. After flow chamber disassembly, slides were washed and fixed with 4% paraformaldehyde for 10 min. Slides were then washed and stained with DAPI. An Olympus FV1000 Confocal Microscope was used to collect images of THP-1 cells bound to endothelial cells. Data are presented as % PKH67+ cells over number of endothelial cells.

2.6. In vivo leukocyte adhesion and rolling in live capillaries

a) *Murine Dorsal Window Chamber Preparation*: Eight week-old C57/BL6 WT male mice were fitted with a dorsal window chamber. The mice window chamber model is widely used for microvascular studies in the unanesthetized state, and the complete surgical technique is described in detail elsewhere [26,27]. Briefly, the animal was prepared for chamber implantation by an IP injection of pentobarbital for anesthesia. Sutures were used to lift the dorsal skin away from the animal, and one frame of the chamber was positioned on the animal's back. A chamber consisted of two identical titanium frames with a 12 mm circular window. With the aid of a stereomicroscope, one side of the skin fold was removed following the outline of the window until only a thin layer of retractor muscle and the intact subcutaneous skin of the opposing side remained. The intact skin of the other side was exposed to the ambient environment. Animals were allowed 2 days for recovery. Finally, catheters (PE-50) were implanted in the carotid artery and jugular vein. Catheters were tunneled under the skin, exteriorized at the dorsal side of the neck, and securely attached to the window frame. Three to four days after the initial surgery, the microvasculature was examined, and only animals passing an established systemic and microcirculatory inclusion criteria entered the study [28,29]. For inclusion criteria, mice were considered suitable for the experiments if: 1) systemic parameters were within normal range. Namely, heart rate (HR) > 400 beat/min, mean arterial blood pressure (MAP) > 80 mmHg, systemic hematocrit (Hct) > 45%, and arterial PO2 pressure > 60 mmHg; and 2) microscopic examination of the tissue in the chamber observed under x650 magnification did not reveal signs of edema or bleeding. For systemic parameters, MAP and heart rate (HR) were recorded continuously (MP 150, Biopac System).

b) *Tourniquet ischemia reperfusion (IR)*: Ischemia was induced for one-hour tourniquet clamp occlusion of the tissue in the window chamber model. Briefly, the periphery of the window was occluded by pressing a thin flat rubber ring (circular clamp). Mice restrained in a Plexiglas tube during ischemia [30]. Flow obstruction was induced by slowly tightening a precision threaded screw fixed to the side of the intact skin of the window chamber. The rubber ring was pressed against the intact skin and towards the cover-glass. Microvascular flow was continuously monitored under trans-illumination, until it ceased in all feeding and draining

microvessels leading in and out of the clamped area without compression injury. The chamber was checked during the clamping period to ensure (no flow) that ischemia was maintained.

c) *Experimental Setup*: The animals were restrained in a tube and the protruding window chamber was fixed to the microscopic stage for trans-illumination (BX51WI, Olympus). Measurements were carried out using a 40X (LUMPFL-WIR, numerical aperture 0.8, Olympus) water immersion objective. Detailed mappings were made of the chamber vasculature so that the same vessels studied at baseline could be followed throughout the experiment. Six to eight arterioles and venules were selected in each preparation. Fields of observation and vessels were chosen for study at locations in the tissue where the vessels were in sharp focus. Leukocyte-endothelium interaction was studied in all the vessels included in the study.

d) *Microhemodynamics*: A video image-shearing method was used to measure vessel diameter (D) [31]. Changes in arteriolar and venular diameter from baseline were used as indicators of a change in vascular tone. Arteriolar and venular centerline velocities were measured on-line using the photodiode cross-correlation method (Photo Diode/Velocity Tracker Model 102B, Vista Electronics). The measured centerline velocity (V) was corrected according to vessel size to obtain the mean RBC velocity [32]. Blood flow (Q) was calculated from the measured values as $Q = \pi \times V\ (D/2)2$.

e) *Functional capillary density (FCD)*: Capillaries were considered functional if red blood cells (RBCs) transit through the capillary segments during a 45 s period. FCD was tabulated from the capillary lengths with RBC transit in an area comprised of 10 successive microscopic fields ($420 \times 320\ \mu m^2$). FCD (cm^{-1}) is the total length of RBC-perfused capillaries divided by the area of the field of view.

f) *Leukocyte-endothelium interaction*: Leukocytes were labeled by intravenous injection of Texas Red anti-CD45 antibodies (10 μg, CalTag, catalog# MCD4517). Fluorescently-labeled leukocytes were excited and images were captured with a Vivid Standard (XF42 filter, Omega Filters) using a low light camera (ORCA 9247, Hamamatsu). Briefly, a straight portion of blood vessels was illuminated for 60 s and video was recorded (10 frames/s). Leukocytes were counted during video playback in a 100 μm length segment and categorized according to their flow behavior as "free-flowing", "rolling" on the endothelium, and "immobilized" cells.

g) *Tissue viability*: Equal volumes of Annexin V (Alexafluor 488 conjugate; Molecular Probes) and propidium iodide (PI, 0.2 mg/mL, Molecular Probes) were mixed, and injected 30 min before visualization by intravital microscopy (8 h after the exchange transfusion). Microscopic images were obtained with a low light video camera (ORCA 9247, Hamamatsu). Labeled cells were counted in the skin fold window and data are given as the average number of fluorescent cells counted in 40 selected visual fields ($210 \times 160\ \mu m$). Sebaceous glands and hair follicles excluded from the cell counts due to their consistently high necrosis and apoptosis rate.

2.7. Statistics

Statistical methods were not used to predetermine necessary sample size, but sample sizes were chosen based on estimates from pilot experiments and previously published results such that appropriate statistical tests could yield significant results. Parametric tests were used that assume normal distribution, which was the case when data were plotted as frequencies. Variances were tested by Levene's test for homogeneity of variance, and variances in the data were not significantly different. Experiments were not performed in a blinded fashion and inclusion/exclusion criteria was not specified at any point. The results are shown as means ± SEM. All statistical analyses were performed by a one-tailed or two-tailed Student's *t*-test or ANOVA, with Bonferroni posthoc unless otherwise indicated; $p < 0.05$ was considered significant. A representative figure for each experiment is presented without combining of data from different batch experiments, unless indicated in the figure legend.

2.8. Study approval

Animal protocols were approved by the Institutional Animal Care and Use Committee (IACUC) at University of California San Diego. All animal procedures were performed in accordance with the IACUC-approved protocols and the research guidelines for the use of laboratory animals of the University of California, San Diego.

3. RESULTS

3.1. CX3CL1-Fc reduces atherosclerotic lesions in a prevention model of atherosclerosis

In initial studies, we assessed the pharmacokinetics of CX3CL1-Fc in *Ldlr* KO mice after a single CX3CL1-Fc IP injection at 30 mg/kg. This dose was chosen based our previous CX3CL1-Fc treatment studies [13]. CX3CL1 levels achieved a Cmax of ~3 nmol/L at 3 h, and plasma levels of 1.85 nmol/L by 72 h (Figure 1A). Using a slightly modified dosing regimen based on our previous studies demonstrating the anti-diabetic effects of CX3CL1-Fc [13], we IP injected 30 mg/kg CX3CL1-Fc twice per week to keep serum levels above ~1.5 nmol/L. *Ldlr* KO mice at 8 weeks of age were fed a Western Diet (WD, 40% fat/1.25% cholesterol) for 4 months and treated with IP saline (VEH) or CX3CL1-Fc injections (Figure 1B). At sacrifice 24 h after the final injection, total serum CX3CL1 levels in CX3CL1-Fc mice were ~2 nmol/L compared with VEH-treated mice at 0.14 nmol/L with no change in body weight or cholesterol (Figure 1C—E). The cholesterol FPLC profiles were relatively similar between CX3CL1-Fc and VEH-treated groups (Figure 1F).

CX3CL1-Fc treatment significantly reduced en face aortic lesion area by 30% (Figure 1G). Analysis of serial sections of the aortic root demonstrated a comparable 30% decrease in lesion area (Figure 1H) and necrotic area within the lesions (Figure 1I) in CX3CL1-Fc-treated *Ldlr* KO mice compared to VEH-treated controls. Interestingly, the decrease in necrotic area in CX3CL1-Fc-treated mice was ~40% compared to the 30% decrease in total lesion area, suggesting that CX3CL1-Fc may play a role in preventing necrosis independent of lesion size (Figure 1H,I AUC). To further analyze plaque stability, we evaluated the α-SMA positive area and collagen content in the aortic root and found a significant increase in the CX3CL1-Fc-treated *Ldlr* KO mice compared to controls (Fig. S1A and S1B). Flow cytometry analyses of aortic wall cell digests showed no change in total macrophages, but a reduction in M1-like polarized macrophages (CD86+) and T lymphocytes (CD3+), with no change in M2-like macrophages (CD206+) in CX3CL1-Fc-treated mice compared with VEH controls (Figure 1J-1M). This shows that CX3CL1-Fc confers changes in immune cell population of lesion areas, as well as a quantitative decrease in lesion size.

In order to rule out potential effects of CX3CL1-Fc on monocyte development, we placed *Ldlr* KO mice on a Western Diet for 1 month during which they were treated with biweekly injections of CX3CL1-Fc or saline (VEH). We then isolated splenocytes and bone marrow cells and conducted flow cytometry, which showed no significant difference in the percentage of CD11b+ Gr-1+ or CD11b+ Gr-1- cell populations of CD45+ live cells between both groups (Fig. S2A and S2B).

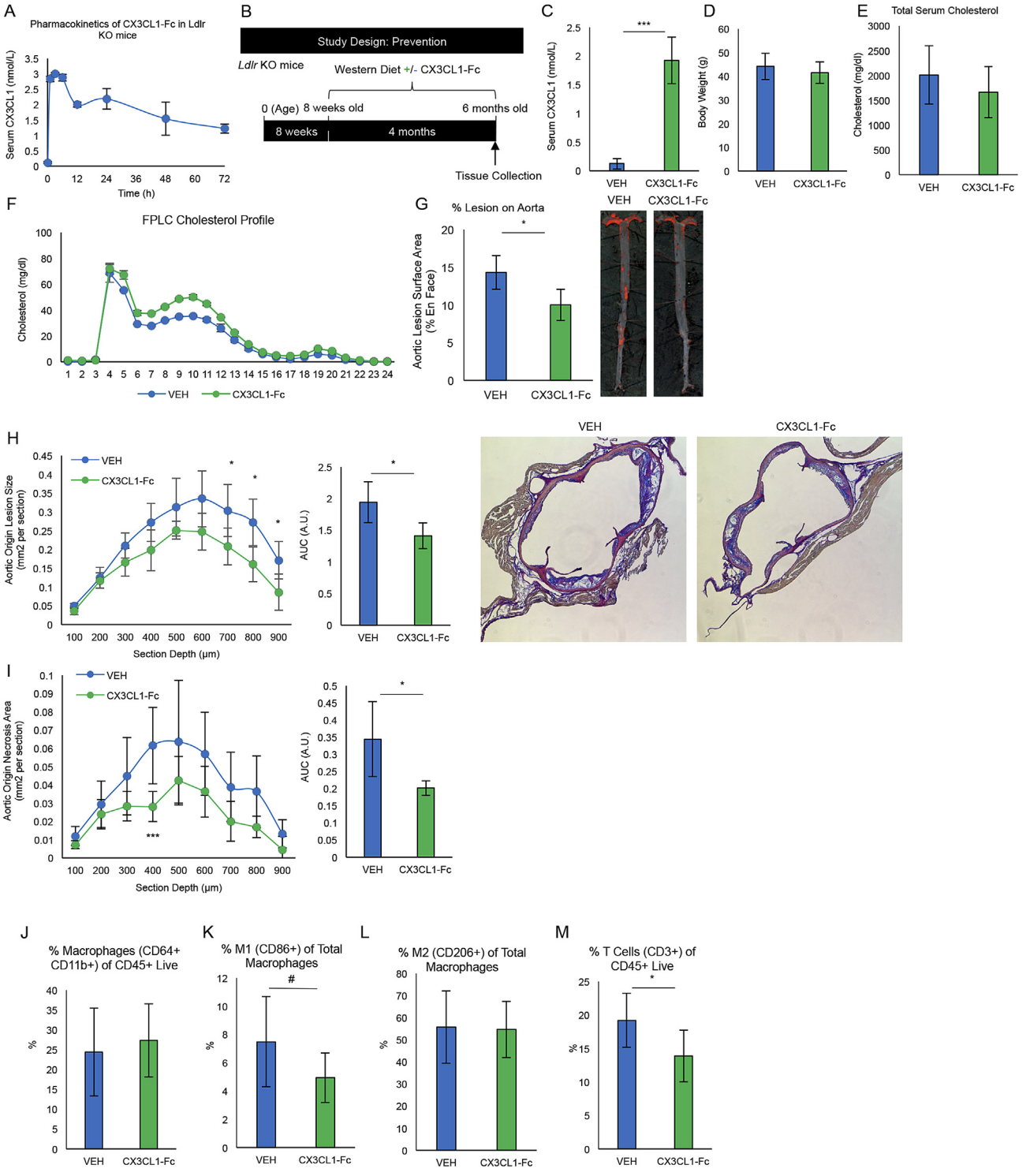

Figure 1: CX3CL1-Fc reduces atherosclerotic lesions in a prevention model of atherosclerosis. (A) Circulating CX3CL1 levels after one injection of CX3CL1-Fc (30 mg/kg) in Ldlr KO mice. After injection, CX3CL1 levels were rapidly increased with stabilization at ~2 nmol/L after 24 h (n = 4). (B) A schematic of prevention study design. CX3CL1-Fc/VEH treatment was started when mice were provided the high-fat/high-cholesterol Western Diet (WD) for 4 months. (C–F) Serum CX3CL1 and lipid content at sacrifice. (C) CX3CL1-Fc-treated mice have ~14 times more serum CX3CL1 in their blood (n = 7–10). Body weight (D), serum cholesterol (E), FPLC cholesterol profile of Ldlr KO mice after 4 months of WD treated with CX3CL1-Fc/VEH (n = 13). (G) En face analysis of total aorta. Percent Sudan IV positive staining over total aortic area in Ldlr KO mice treated with CX3CL1-Fc/VEH, representative images are shown (n = 4–7). Cross-sectional aortic root analyses of lesion size (H) and necrotic area within lesions (I), representative images are shown to the right (n = 4–7). AUC, area under the curve. A.U., arbitrary unit. (J–M) Flow cytometry analysis of aortic cell digests showed no difference the in percentage of macrophages of CD45+ Live cells (J). However, there was a decrease in CD86+ M1-like polarized macrophages (K) and no change in CD206+ M2-like polarized macrophages (L) as a percent of total macrophages (CD64+ CD11b+) in mice treated with CX3CL1-Fc (n = 9). Also, a decrease in CD3+ T cells (M) as a percent of CD45+ Live cells was observed in aortic cell digests of CX3CL1-Fc treated mice (n = 9). Data are presented as mean ± SEM. #$p < 0.05$ (one-tailed t-test). For all panels, values are mean ± SD. *$p < 0.05$ and ***$p < 0.001$.

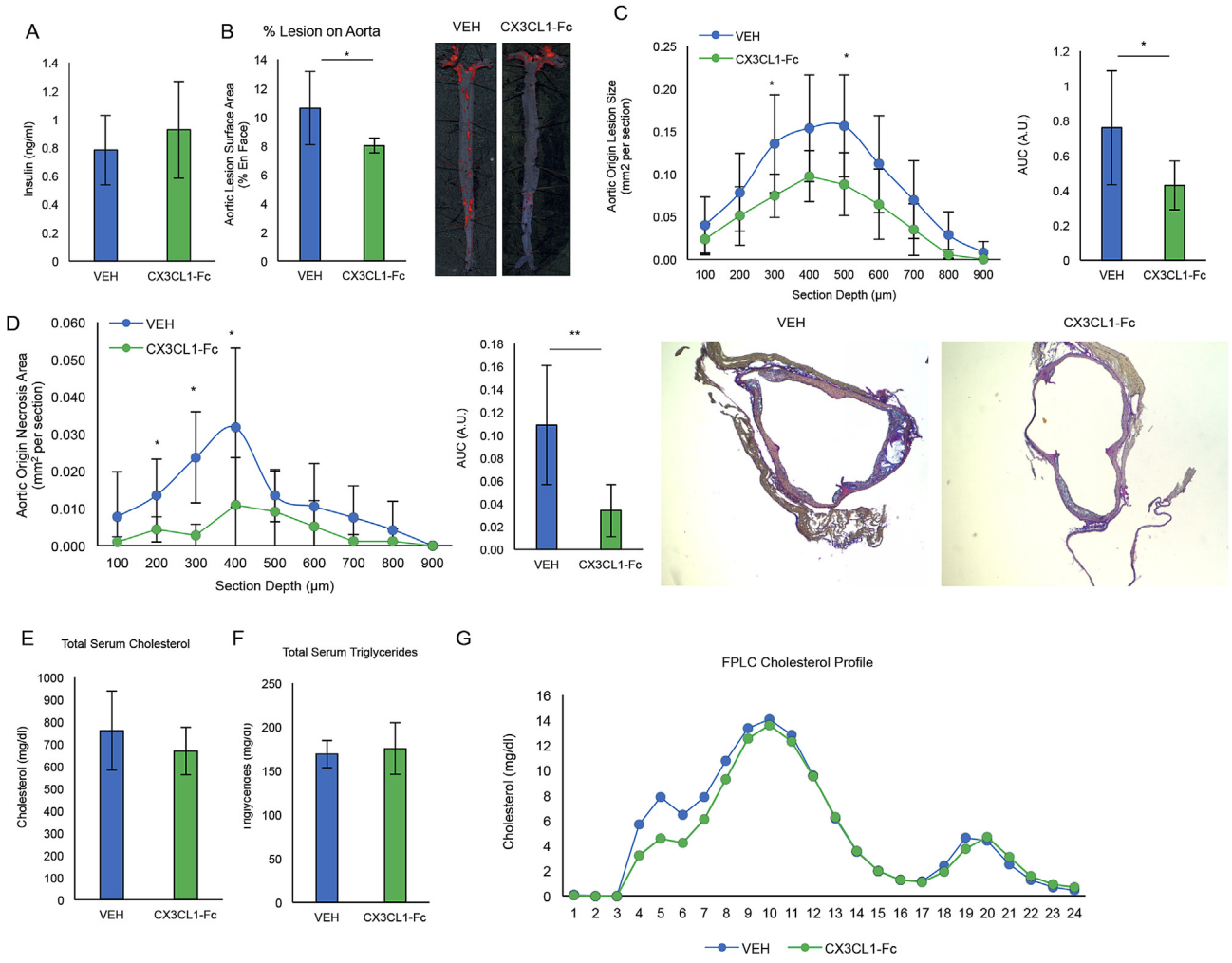

Figure 2: CX3CL1-Fc reduces atherosclerosis in *Ldlr* KO mice independent of improving glucose tolerance. Under the same scheme as Figure 1 except for use of a high-cholesterol (1.25%)/low-fat (4.4%) diet, (A) insulin levels are unchanged between CX3CL1-Fc and VEH-treated Ldlr KO mice (n = 8). (B) En face analysis of total aorta. CX3CL1-Fc-treated Ldlr KO mice had significantly less aortic lesion area on the aortic surface. Representative images are shown below (n = 8). (C–D) Sections of the aortic root show decreased lesion size (C) and decreased necrotic area (D) in mice treated with CX3CL1-Fc compared to controls visualized as area under the curve. Representative images are shown (n = 8). (E–G) Serum lipid contents. Total serum cholesterol (E), triglycerides (F) and FPLC cholesterol profile (G) show no difference between CX3CL1-Fc-treated and VEH-treated mice (n = 8). For all panels, data are presented as mean ± SD. *p < 0.05 and **p < 0.01.

We also found no significant difference in the percentage of CD11b+ F4/80+ or CD11b+ F4/80- cell populations of CD45+ live cells between both groups (Fig. S2A and S2B). This suggests that CX3CL1-Fc did not affect monocyte/macrophage development in the context of these in vivo studies.

We next sought to determine the impact of inhibiting CX3CL1-mediated monocyte recruitment on established lesions. *Ldlr* KO mice were fed a WD for 4 months and then divided into 3 cohorts: cohort 1 was sacrificed for the determination of "baseline" atherosclerosis, while cohorts 2 and 3 were continued on the WD for an additional 4 months. During these final 4 months, cohort 2 was treated with CX3CL1-Fc and cohort 3 received VEH (Fig. S3A) with atherosclerosis analyses following treatment. As expected, both cohorts 2 and 3 had a greater extent of atherosclerosis than observed for cohort 1, but there were no differences in body weight, en face aortic lesion size or aortic root lesions between cohort 2 and 3 at the end of study (Fig. S3B–S3D). There were also no differences observed between cohort 2 and 3 in total macrophages, nor in M1-like or M2-like macrophages in carotid wall digests (Fig. S3E–S3G). T cells were also unchanged in both carotid wall digests and lymph nodes (Fig. S3H–S3I). Finally, under these conditions, CX3CL1-Fc had no effect on Tissue-Resident Memory T cell (TRM) populations in the spleen, lymph nodes or carotid arteries (Fig. S4A–S4B).

3.2. CX3CL1-Fc reduces atherosclerosis in *Ldlr* KO mice in the absence of insulin resistance

Insulin resistance and hyperglycemia have been implicated as pro-atherogenic risk factors [33]. Recently, we reported that chronic CX3CL1-Fc treatment improves glucose tolerance in obese and insulin resistant rodent models, raising the question as to whether any of the anti-atherosclerosis effects of chronic CX3CL1-Fc therapy were mediated by enhancing insulin action and glycemic control [22]. It has been previously shown that a high cholesterol (1%)/low fat (4.4%) diet (HCD) can induce atherosclerosis in *Ldlr* KO mice without the concomitant obesity and glucose intolerance that occurs with the WD [34]. Therefore, to determine whether the anti-atherosclerosis effects of CX3CL1-Fc were independent of the beneficial effects of CX3CL1-Fc on glucose tolerance, we followed the same protocol as in Figure 1, but

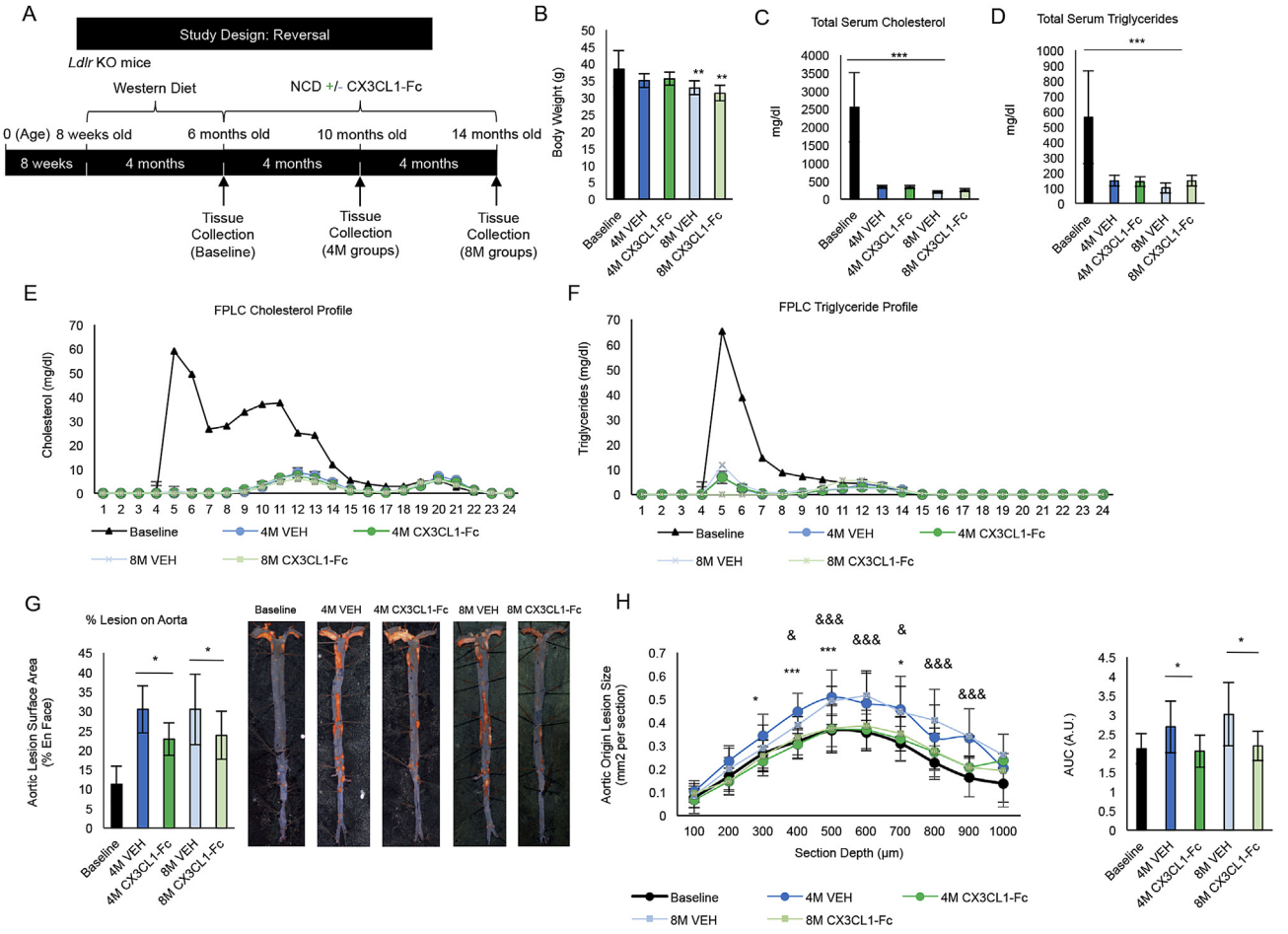

Figure 3: CX3CL1-Fc administration reduces atherosclerosis after diet switch. (A) A schematic of the diet switch study. CX3CL1-Fc injections began after switch from 4 months of WD to normal chow diet (NCD). (B) Body weight of baseline mice are significantly higher than 8 month mice after diet switch (n = 8–10). (C–F) Serum lipid analyses. Total serum cholesterol (C) and triglycerides (D) are significantly decreased in mice that are switched from WD to NCD with no differences between CX3CL1-Fc-treated mice and controls (n = 6–9). FPLC profiles of cholesterol (E) and triglycerides (F) show a decrease in 4 and 8 month diet switch mice with no difference between CX3CL1-Fc and VEH controls (Data are a pool of serum from 8 mice). (G) En face analysis of total aorta. Aortic lesion area is reduced in CX3CL1-Fc-treated mice compared to controls at 4 and 8 months after diet switch. Representative images are shown on the right (n = 7–10). (H) Cross-sectional analysis of aortic root area. Aortic root sections shown as area under the curve have significantly less lesion area in CX3CL1-Fc mice at 4 and 8 months after diet switch (n = 7–12). AUC, area under the curve. A.U., arbitrary unit. In all panels, data are presented as mean ± SD. */& $p < 0.05$, **/&& $p < 0.01$, ***/&&& $p < 0.001$. In (H), * denotes significance between 4M VEH and 4M CX3CL1-Fc, while & denotes significance between 8M VEH and 8M CX3CL1-Fc.

fed mice a HCD instead. Insulin levels were the same in *Ldlr* KO mice fed normal chow or HCD diet and after 4 months of CX3CL1-Fc treatment, insulin levels were ~0.8 ng/ml, regardless of CX3CL1-Fc or VEH treatment (Figure 2A). This serum insulin level is in line with other reports of normal chow-fed *Ldlr* KO or C57/Bl6 mice [35,36]. *Ldlr* KO mice fed a HCD showed a significant ~25% reduction in aortic lesion area (Figure 2B), with a ~40% decrease across the aortic root (Figure 2C). Necrosis area in the aortic root was significantly reduced with a concomitant increase in α-SMA positivity in mice treated with CX3CL1-Fc compared to controls (Figure 2D and Fig. S1B). No change in collagen was observed between the groups (Fig. S1A). Total plasma cholesterol (Figure 2D) and triglyceride (Figure 2E) levels were comparable between the 2 groups, but the absolute levels were lower than observed with the WD. In addition, the cholesterol FPLC profiles were similar between both the CX3CL1-Fc and VEH group under this diet regiment (Figure 2F). These results show that CX3CL1-Fc can prevent atherosclerosis independent of glucose intolerance and pronounced hypercholesterolemia.

3.3. CX3CL1-Fc reduces atherosclerosis after WD diet switch

To further understand the effects of the CX3CL1-Fc intervention on atherosclerosis, a model of atherosclerosis after diet switch was studied, in which *Ldlr* KO mice were fed a WD for 4 months then switched to a normal chow diet (NCD). At the time of diet switch from WD to NCD, the mice were treated with CX3CL1-Fc or VEH for 4 or 8 additional months (Figure 3A). As expected, baseline mice (*Ldlr* KO mice fed a WD for 4 months) showed increased body weight (Figure 3B) compared with either CX3CL1-Fc or VEH mice at both 4 months and 8 months after the diet switch. The FPLC cholesterol and triglyceride profiles were not different between CX3CL1-Fc or VEH groups at either 4 and 8 months, though obviously different than those of mice at baseline on WD (Figure 3C,D). It is of interest that, after diet switch, circulating cholesterol and triglyceride levels normalize (Figure 3E,F). Despite this, atherosclerosis, as assessed by lesion area, continues to progress, consistent with previous reports (Figure 3G) [37,38]. In contrast, compared to the 4M and 8M VEH controls, CX3CL1-Fc treatment led to a significant ~25% decrease in lesion

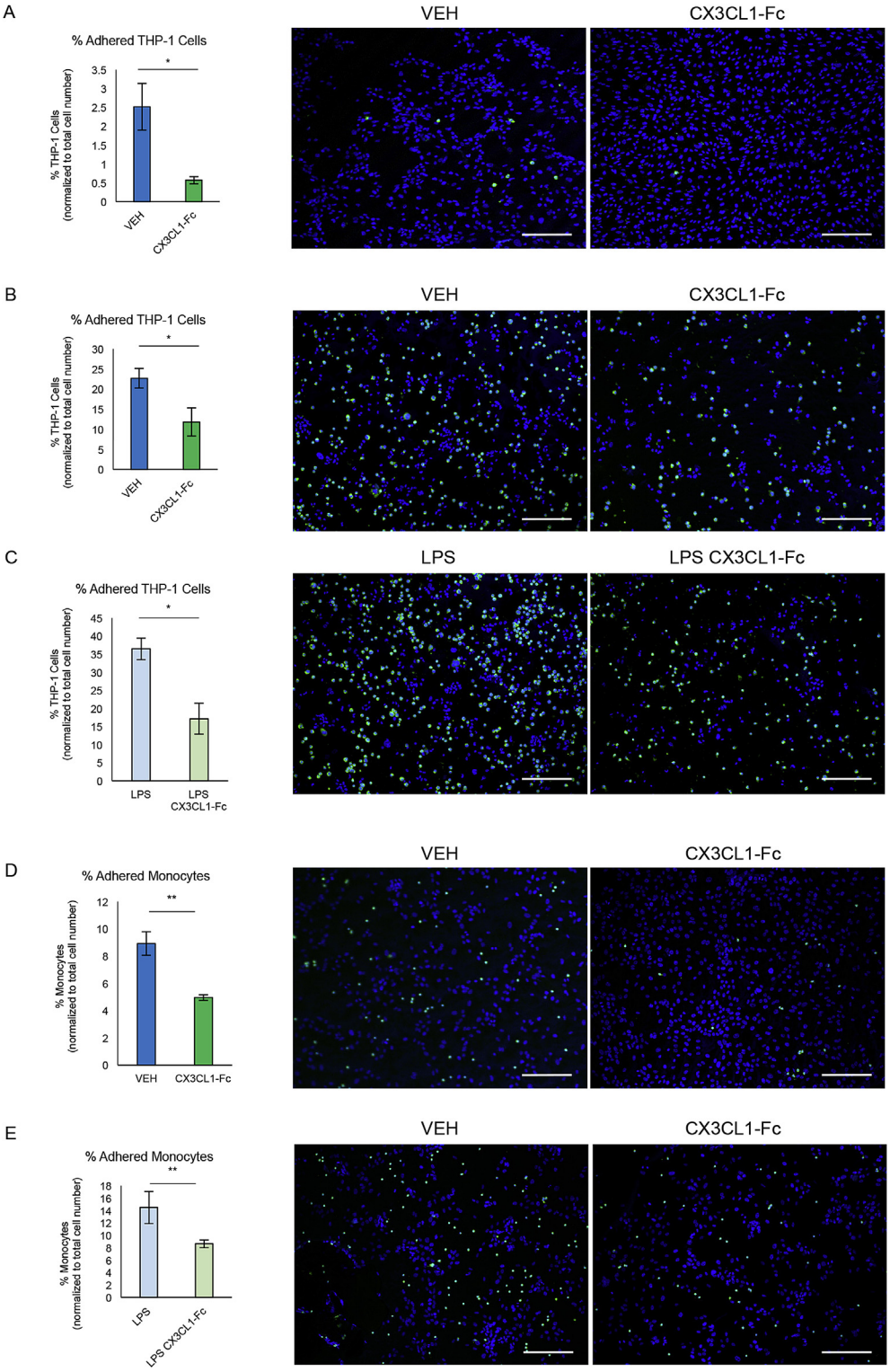

Figure 4: CX3CL1-Fc reduces monocyte cell adhesion to endothelial monolayers. (A) In vitro THP-1 adhesion assay under flow conditions. THP-1 cells pre-treated with CX3CL1-Fc are significantly less adherent to a HUVEC monolayer when under a shear stress of 1 dyne/cm^2 compared to VEH-treated controls. Representative images are shown (n = 3). (B–C) Static in vitro THP-1 adhesion assays. CX3CL1-Fc pre-treatment of THP-1 cells leads to reduced adhesion to a HUVEC monolayer under normal (B) and LPS-stimulated conditions (C). Representative images are shown (n = 3). (D–E) Static in vitro peripheral blood monocyte adhesion assays. Peripheral blood monocytes pre-treated with CX3CL1-Fc are less adherent to a HUVEC monolayer under normal (D) and LPS-stimulated (E) conditions. Representative images are shown (n = 3). Monocytes are shown in green and nuclei are labeled with DAPI. Scale bar = 100 μm. Data in both panels are presented as mean ± SD. *p < 0.05.

area after both 4 and 8 months of treatment (Figure 3G). A similar increase in aortic root lesion area was observed in 4M and 8M VEH-treated mice (Figure 3H). In contrast, a dramatic inhibition of progression of lesion formation was observed at the aortic root in CX3CL1-Fc-treated mice at both 4M and 8M. Absolute lesion areas were equal to that observed in mice at the 4 month baseline period, prior to treatment (Figure 3H). Thus, initiating CX3CL1-Fc treatment at the time of the diet switch completely prevented the subsequent progression of atherosclerosis lesions at the aortic root and attenuated the continued progression observed in the aorta. Since the CX3CL1-Fc group exhibited much less atherosclerosis progression after the diet switch, this indicates that CX3CL1-Fc caused atheroprotective effects that were cholesterol independent.

To characterize the quality of immune cell populations, we harvested cells for flow cytometry analysis from *Ldlr* KO mice fed a WD for 4 months then switched to NCD after 4 months, while treated with CX3CL1-Fc or VEH. In carotid cell digests, we observed no difference in the percentage of macrophages or percentage of T cells in CD45+ live cells, nor any differences in M1-like or M2-like macrophages as a percentage of total macrophages (Fig. S5A). Furthermore, in lymph nodes and splenocytes, there were no differences observed between the groups in the percentage of T cells of CD45+ live (Fig. S5B and S5C). This diet-switch study shows that CX3CL1-Fc significantly decreases aortic lesion size, consistent with the prevention study results (Figure 1). However, immune cell populations were not affected, perhaps due to the greater effect of the lesion size.

3.4. CX3CL1-Fc reduces monocyte adhesion under flow and static conditions

To assess the ability of CX3CL1-Fc to block monocyte binding to endothelial cells, we used an in vitro system to measure the binding of human THP-1 cells to a HUVEC layer under flow and static conditions. As seen in Figure 4A, THP-1 cells incubated with CX3CL1-Fc for 30 min prior to 1 dyne/cm^2 flow over a HUVEC monolayer led to significantly fewer adhered THP-1 cells. To confirm these results, static monocyte adhesion assays were conducted in 24-well plates. Pretreating THP-1 cells for 30 min with CX3CL1-Fc reduced adhesion to a HUVEC monolayer by 50% (Figure 4B). Prior treatment of HUVECs with LPS (100 ng/ml for 30 min) led to an increase in THP-1 cell binding while concomitant pre-treatment with CX3CL1-Fc completely prevented this effect (Figure 4C). Similar results were observed when murine peripheral blood monocytes were used instead of THP-1 cells (Figure 4D–E).

3.5. CX3CL1-Fc prevents in vivo leukocyte adhesion and rolling

To translate our in vitro monocyte adhesion studies to the in vivo situation, we used a dorsal window chamber model (DWCM) to study murine microvascular dynamics [39]. This chamber provides a method to control the blood supply into the 'windowed' skin area, allowing analysis of blood cell dynamics after IR injury. To test the effect of CX3CL1-Fc administration on leukocyte binding to the stressed vessel wall, DWCM-fitted wild-type C57/BL6 mice were exposed to local skin ischemia for 1 h, followed by blood reperfusion and concomitant intravenous injection of 30 mg/kg CX3CL1-Fc or VEH via the carotid artery. Leukocytes and other cells within the skin microvasculature were visualized by microscopy and quantified over 24 h. In CX3CL1-Fc-treated mice, the number of adherent and rolling leukocytes on the capillary vascular wall was significantly decreased at 30 min, 2 h and 24 h after reperfusion compared to VEH-treated controls (Figure 5A–B). This was accompanied by increased venous blood flow and functional capillary density (Figure 5C–D). No changes in mean arterial pressure or heart rate were detected (Figure 5E–F). After the 24 h measurement was made, fluorescently labeled annexin V antibodies and propidium iodide were injected into the window chambers of CX3CL1-Fc or VEH treated mice in order to label apoptotic or necrotic cells, respectively. Confocal microscopy analyses from 40 different fields in the insulted skin area showed that CX3CL1-Fc treated mice exhibited significantly reduced apoptosis (number of annexin V labeled cells, Figure 5G) and necrosis (number of propidium iodide labeled cells, Figure 5H).

4. DISCUSSION

The current studies show that chronic treatment of *Ldlr* KO mice with a long acting CX3CL1-Fc fusion protein (and CX3CR1 agonist) led to a significant decrease in atherosclerotic lesions in the context of both disease progression and diet switch. This occurred without a change in plasma cholesterol levels. CX3CL1-Fc interfered with monocyte binding to HUVEC cells in vitro and reduced leukocyte rolling/adhesion in murine vessels in vivo. These changes were associated with decreased aortic wall M1-like macrophages and T cells, which would be expected to further decrease the chronic inflammatory milieu in the lesions. These results indicate that treatment with a long-acting CX3CR1 agonist prevents monocytes from adhering to the endothelial wall, thus, reducing atherosclerosis.

Monocyte/macrophages are the major leukocyte subset in atherosclerotic plaques [40] and depletion of these cells reduces atherosclerotic lesion area [41]. Many studies have implicated monocyte adhesion to the endothelium as a necessary step in the development of atherosclerosis [8,42]. Therefore, inhibiting monocyte-endothelial cell interactions should be atheroprotective. CX3CL1 is a cell membrane spanning ligand and the extracellular domain interacts with CX3CR1 on circulating monocytes to promote monocyte-endothelial cell adhesion. As well, activation of CX3CR1 can enhance monocyte-endothelial cell adhesion and transmigration by inducing expression of other adhesion molecules [43].

Ldlr or *ApoE* KO mice with either CX3CL1 or CX3CR1 KO exhibit reduced atherosclerosis and lesion monocytes/macrophages [16,18,44,45]. Moreover, it has been shown that competitive inhibition of CX3CR1 by an antagonist reduces the progression of atherosclerosis in both *ApoE* and *Ldlr* KO mice [46]. In the present studies, we utilized a novel approach by treating mice with a long acting CX3CR1 agonist rather than an antagonist. Since KOs of CX3CR1 or CX3CL1 are atheroprotective due to reduced monocyte-endothelial cell interactions, we reasoned that large amounts of extracellular CX3CL1-Fc would both agonize the CX3CR1 receptor and interfere with the normal interactions between monocytes and endothelial cells. Agonizing CX3CR1 avoids monocyte cell death associated with blocking CX3CL1-CX3CR1 signaling, while the decoy feature prevents monocyte-endothelial cell adhesion necessary for atherosclerosis [47]. As predicted, in vitro treatment with CX3CL1-Fc prevented monocyte adhesion to a HUVEC monolayer under normal and pro-inflammatory conditions. Moreover, using in vivo DWCM studies, we found that leukocyte adhesion/rolling on the endothelial lining of living mice was significantly decreased after treatment with CX3CL1-Fc compared with VEH-treated controls. Importantly, *Ldlr* KO mice treated with CX3CL1-Fc showed significantly reduced atherosclerotic lesions in both prevention and diet switch models of atherosclerosis. Since CX3CL1-Fc treatment can also stimulate CX3CR1 receptor signaling in circulating blood monocytes, our results suggest that circulating monocyte recruitment to the endothelial wall relies largely on the physical interaction between CX3CL1 and CX3CR1. Therefore, while the results

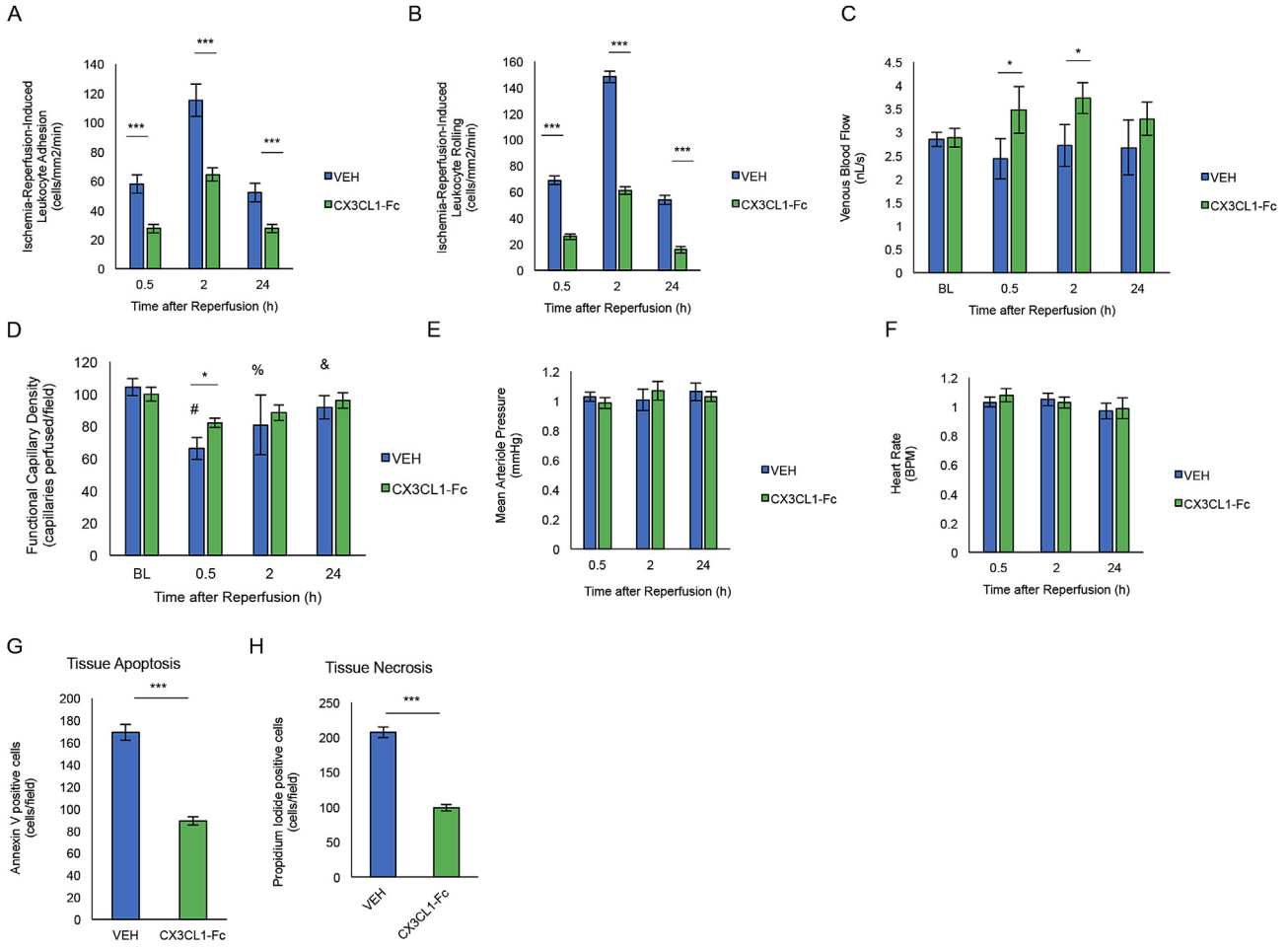

Figure 5: CX3CL1-Fc administration prevents in vivo leukocyte adhesion and rolling on the vascular wall. A dorsal window chamber model was used to visualize leukocytes traveling through capillaries in vivo. (A—B) C57/BL6 male mice treated with CX3CL1-Fc (30 mg/kg) for 30 min prior to 1 h of local ischemia had significantly fewer leukocytes adhered (A) and rolling (B) along the capillaries of the dorsal skin at 0.5 h, 2 h and 24 h after reperfusion ($n = 4$). (C) Venous blood flow was significantly increased in CX3CL1-fc-treated mice compared with VEH after 0.5 h and 2 h after reperfusion ($n = 4$). (D) Functional capillary density as a measurement by perfused capillaries after ischemia-reperfusion was significantly increased in CX3CL1-Fc-treated mice compared with controls ($n = 4$). (E—F) Mean arterial pressure (E) and heart rate (F) in mice treated with CX3CL1-Fc or VEH ($n = 4$). (G—H) Tissue apoptosis (G) and necrosis (H) was significantly reduced in CX3CL1-Fc treated mice ($n = 4$). Data are presented as mean ± SD. *$p < 0.05$ **$p < 0.01$ and ***$p < 0.001$. In (D), # denotes $p < 0.05$ between 0.5 h and baseline, % denotes $p < 0.05$ between 2 h and baseline and & notes $p < 0.05$ between 24 h and 0.5 h after Bonferroni posthoc test.

support previous data illustrating the role of CX3CR1-CX3CL1 interactions in monocyte adhesion and atherosclerosis progression, they also provide important new evidence showing that a long acting CX3CL1 agonist can block monocyte-endothelial interactions and improve atherosclerosis. It is important to note that since CX3CL1-Fc treatment is associated with significantly reduced lesion size, this would mean that absolute number of aortic wall macrophages would be decreased. The relevance of this to human atherosclerosis is suggested by the observation that CX3CL1 is expressed in human carotid artery plaques in all stages of atherosclerosis [17] and that loss-of-function variants of the human *CX3CR1* gene (with decreased CX3CL1 binding affinity) are associated with reduced CVD [19].

We utilized 3 separate protocols to assess the effects of CX3CL1-Fc treatment on atherosclerosis. In the mode of prevention (concomitant onset of treatment and WD) and reversion (onset of CX3CL1-Fc treatment at the time of cholesterol lowering due to the WD to chow switch), CX3CL1-Fc was highly efficacious at reducing atherosclerosis. However, with established atherosclerosis (treatment study), CX3CL1-Fc was without beneficial effects in the context of sustained and marked hypercholesterolemia (Fig. S3). The efficacy of CX3CL1-Fc treatment may be restricted to conditions whereby ongoing monocyte recruitment is necessary to influence disease status. In this case, monocyte adhesion may be most important at the beginning and termination of WD. In the treatment mode, monocytes have already infiltrated the vessel wall to become foam cells and this may explain why CX3CL1-Fc was ineffective since its anti-atherosclerosis effects are cell adhesion-dependent. Indeed, previous studies suggest that the macrophage contribution to established lesions is due primarily to in situ proliferation rather than monocyte recruitment [48]. By contrast, during early atherosclerosis, monocyte recruitment has a more profound role [48]. In the diet switch study, we observed increased atherosclerosis progression in the VEH mice at 4 and 8 months compared to baseline. This result has been observed by other groups [37,38]. Interestingly, significant remodeling occurs soon after the diet switch, which involves changes in macrophages, T cells and neutrophils in the atherosclerotic lesions [37]. This is consistent with our proposed mechanism that CX3CL1-Fc has anti-atherosclerosis effects when lesions are cell adhesion-dependent. Consistent with these

observations in mice, regression of atherosclerosis takes a long period of time after a cholesterol-lowering regimen. There may also be effects related to T cells but our current study does not explore this. These current results show that CX3CL1-Fc improves atherosclerosis in a cholesterol-independent manner, raising the possibility that the use of a long acting soluble CX3CL1 could provide an additive anti-atherosclerosis efficacy additive to cholesterol-lowering drugs such as statins.

Of interest, chronic CX3CL1-Fc administration reduced the necrotic core area in aortic root cross sections. The magnitude of this effect on necrotic area was ~10% greater than the effect of CX3CL1-Fc on total lesion size suggesting that it is not simply due to decreased plaque formation in CX3CL1-Fc treated mice. In the process of atherosclerosis, early stage fatty streaks can develop into fibroatheroma with a cell-free, lipid-rich necrotic core. Increased apoptosis of the infiltrated macrophages and vascular smooth muscle cells contributes to the expansion of this necrotic core. This feature of atherosclerotic lesions can cause plaque instability and plaque rupture which is a major trigger for life-threatening acute coronary events. The effect of CX3CL1-Fc treatment to increase plaque content of collagen and α-SMA is consistent with improved plaque stability. Recently, Zhao et al. have shown that CX3CR1 activation suppresses apoptosis in macrophages and vascular smooth muscle cells [49], whereas, CX3CR1 inhibition decreases monocyte survival [46,50]. It is likely that the proinflammatory immune cells, which propagate within atherosclerotic areas, facilitate necrosis of cells within these lesions and this is a well-known contributor to plaque rupture and instability [51]. Our findings that CX3CL1-Fc treatment leads to decreased apoptosis and necrosis in the IR model, along with decreased areas of necrosis within the remaining aortic atherosclerotic lesions, raises the possibility that treatment with CX3CL1-Fc may lead to stabilization of existing plaques, as well as prevention of their development. However, it should be noted that the IR model is different from hypercholesterolemia-induced insults, and this should be further investigated.

Our previous studies demonstrated that CX3CL1-Fc treatment improves glucose metabolism and insulin sensitivity in high-fat diet-induced obese mice [22]. In the current study, we have shown that CX3CL1-Fc reduces atherosclerosis even in cohorts of HCD-fed *Ldlr* KO mice that do not have glucose intolerance (Figure 2) [34]. This combination of therapeutic benefits makes CX3CL1-Fc an interesting candidate for potential treatment of T2DM. Indeed, poor glycemic control is associated with increased CVD risk [52], and many studies have shown that high glucose or high fat can promote a pro-atherogenic state in endothelial cells [53]. CX3CL1-Fc is unique in that it has a direct beneficial effect on beta cell function, insulin sensitivity, and atherosclerosis, which could be an advantage over current treatment modalities. However, since CX3CL1 can lead to platelet activation and aggregation, the potential for thrombosis should be considered in future translational studies [54–56]. Thus, using our approach with a circulating CX3CR1 agonist, one can harness the beneficial anti-diabetic effects to the atheroprotective effects shown here and this could provide a clinical advantage.

In summary, treatment of *Ldlr* KO mice with CX3CL1-Fc interferes with native CX3CR1-CX3CL1 interactions, leading to reduced lesion immune cell accumulation, less atherosclerotic lesions and decreased necrotic core area. This occurred in both prevention and diet-switch models of atherosclerosis. Therefore, it is possible that soluble CX3CL1 administration is not only protective from early atherosclerosis, but also beneficial for managing late stage atherosclerosis. Coupled with our earlier results showing the metabolic benefit of CX3CL1-Fc treatment on glucose homeostasis [22], long acting soluble CX3CL1-Fc treatment may ultimately find a role in our therapeutic armamentarium.

SOURCES OF FUNDING

This research was supported from grants awarded by the US National Institute of Diabetes and Digestive and Kidney Diseases (DK074868, DK063491, and DK101395), National Heart, Lung, and Blood Institute (HL088093 awarded to J.L.W.) and a UCSD/UCLA Diabetes Research Center P&F grant. MR is supported by a postdoctoral fellowship from the American Heart Association (16POST29990015). This work was also supported by a grant from Takeda California, Inc.

FINANCIAL DISCLOSURES

RDJ, SP, DB, JB, and, AF are employed by Takeda California, Inc. MW was employed by Takeda California Inc., but is now employed by Genentech. AP was employed by Takeda California Inc., but is now employed by Seal Rock Therapeutics, Inc. RDJ was employed by Takeda California Inc., but is now the principal at Ron de Jong Consulting, LLC. YSL and JMO have received past research funding from Takeda California Inc. JLW is a consultant for Ionis Pharmaceuticals and has patents covering the commercial use of oxidation-specific epitopes held by the University of California. CX3CL1/CX3CR1 and related methods of use reported in this study are covered in patent 9764001 by J.M.O and Y.S.L.

ACKNOWLEDGEMENTS

We thank Cynthia Walser for surgical instrumentation of animals for the DWCM experiment.

CONFLICT OF INTEREST

None declared.

APPENDIX A. SUPPLEMENTARY DATA

Supplementary data to this article can be found online at https://doi.org/10.1016/j.molmet.2018.11.011.

REFERENCES

[1] Benjamin, E.J., Blaha, M.J., Chiuve, S.E., Cushman, M., Das, S.R., Deo, R., et al., 2017. Heart disease and stroke statistics-2017 update: a report from the American heart association. Circulation 135:e146–e603.

[2] Perak, A.M., Ning, H., de Ferranti, S.D., Gooding, H.C., Wilkins, J.T., Lloyd-Jones, D.M., 2016. Long-term risk of atherosclerotic cardiovascular disease in US adults with the familial hypercholesterolemia phenotype. Circulation 134: 9–19.

[3] Lovren, F., Teoh, H., Verma, S., 2015. Obesity and atherosclerosis: mechanistic insights. Canadian Journal of Cardiology 31:177–183.

[4] Mackey, R.H., Mora, S., Bertoni, A.G., Wassel, C.L., Carnethon, M.R., Sibley, C.T., et al., 2015. Lipoprotein particles and incident type 2 diabetes in the multi-ethnic study of atherosclerosis. Diabetes Care 38:628–636.

[5] Brener, M.I., Post, W.S., Haberlen, S.A., Zhang, L., Palella Jr., F.J., Jacobson, L.P., et al., 2016. Comparison of insulin resistance to coronary atherosclerosis in human immunodeficiency virus infected and uninfected men (from the multicenter AIDS cohort study). The American Journal of Cardiology 117:993–1000.

[6] Singh, R.B., Mengi, S.A., Xu, Y.J., Arneja, A.S., Dhalla, N.S., 2002. Pathogenesis of atherosclerosis: a multifactorial process. Experimental and Clinical Cardiology 7:40–53.
[7] Hansson, G.K., 2005. Inflammation, atherosclerosis, and coronary artery disease. New England Journal of Medicine 352:1685–1695.
[8] Swirski, F.K., Pittet, M.J., Kircher, M.F., Aikawa, E., Jaffer, F.A., Libby, P., et al., 2006. Monocyte accumulation in mouse atherogenesis is progressive and proportional to extent of disease. Proceedings of the National Academy of Sciences of the United States of America 103:10340–10345.
[9] Soehnlein, O., Drechsler, M., Doring, Y., Lievens, D., Hartwig, H., Kemmerich, K., et al., 2013. Distinct functions of chemokine receptor axes in the atherogenic mobilization and recruitment of classical monocytes. EMBO Molecular Medicine 5:471–481.
[10] Ley, K., Miller, Y.I., Hedrick, C.C., 2011. Monocyte and macrophage dynamics during atherogenesis. Arteriosclerosis Thrombosis and Vascular Biology 31: 1506–1516.
[11] Ley, K., Laudanna, C., Cybulsky, M.I., Nourshargh, S., 2007. Getting to the site of inflammation: the leukocyte adhesion cascade updated. Nature Reviews Immunology 7:678–689.
[12] Clark, A.K., Staniland, A.A., Malcangio, M., 2011. Fractalkine/CX3CR1 signalling in chronic pain and inflammation. Current Pharmaceutical Biotechnology 12:1707–1714.
[13] Lee, Y.S., Morinaga, H., Kim, J.J., Lagakos, W., Taylor, S., Keshwani, M., et al., 2013. The fractalkine/CX3CR1 system regulates beta cell function and insulin secretion. Cell 153:413–425.
[14] Ancuta, P., Rao, R., Moses, A., Mehle, A., Shaw, S.K., Luscinskas, F.W., et al., 2003. Fractalkine preferentially mediates arrest and migration of CD16+ monocytes. Journal of Experimental Medicine 197:1701–1707.
[15] Darbandi-Tehrani, K., Hermand, P., Carvalho, S., Dorgham, K., Couvineau, A., Lacapere, J.J., et al., 2010. Subtle conformational changes between CX3CR1 genetic variants as revealed by resonance energy transfer assays. The FASEB Journal 24:4585–4598.
[16] Combadiere, C., Potteaux, S., Gao, J.L., Esposito, B., Casanova, S., Lee, E.J., et al., 2003. Decreased atherosclerotic lesion formation in CX3CR1/apolipoprotein E double knockout mice. Circulation 107:1009–1016.
[17] Stolla, M., Pelisek, J., von Bruhl, M.L., Schafer, A., Barocke, V., Heider, P., et al., 2012. Fractalkine is expressed in early and advanced atherosclerotic lesions and supports monocyte recruitment via CX3CR1. PLoS One 7: e43572.
[18] Teupser, D., Pavlides, S., Tan, M., Gutierrez-Ramos, J.C., Kolbeck, R., Breslow, J.L., 2004. Major reduction of atherosclerosis in fractalkine (CX3CL1)-deficient mice is at the brachiocephalic artery, not the aortic root. Proceedings of the National Academy of Sciences of the United States of America 101:17795–17800.
[19] McDermott, D.H., Fong, A.M., Yang, Q., Sechler, J.M., Cupples, L.A., Merrell, M.N., et al., 2003. Chemokine receptor mutant CX3CR1-M280 has impaired adhesive function and correlates with protection from cardiovascular disease in humans. Journal of Clinical Investigation 111:1241–1250.
[20] Karlmark, K.R., Zimmermann, H.W., Roderburg, C., Gassler, N., Wasmuth, H.E., Luedde, T., et al., 2010. The fractalkine receptor CX(3)CR1 protects against liver fibrosis by controlling differentiation and survival of infiltrating hepatic monocytes. Hepatology 52:1769–1782.
[21] Aoyama, T., Inokuchi, S., Brenner, D.A., Seki, E., 2010. CX3CL1-CX3CR1 interaction prevents carbon tetrachloride-induced liver inflammation and fibrosis in mice. Hepatology 52:1390–1400.
[22] Riopel, M., Seo, J.B., Bandyopadhyay, G.K., Li, P., Wollam, J., Chung, H., et al., 2018. Chronic fractalkine administration improves glucose tolerance and pancreatic endocrine function. Journal of Clinical Investigation.
[23] Palinski, W., Ord, V.A., Plump, A.S., Breslow, J.L., Steinberg, D., Witztum, J.L., 1994. ApoE-deficient mice are a model of lipoprotein oxidation in atherogenesis. Demonstration of oxidation-specific epitopes in lesions and high titers of autoantibodies to malondialdehyde-lysine in serum. Arteriosclerosis and Thrombosis 14:605–616.
[24] Douglas, R.M., Bowden, K., Pattison, J., Peterson, A.B., Juliano, J., Dalton, N.D., et al., 2013. Intermittent hypoxia and hypercapnia induce pulmonary artery atherosclerosis and ventricular dysfunction in low density lipoprotein receptor deficient mice. Journal of Applied Physiology (1985) 115: 1694–1704.
[25] Wang, K.C., Yeh, Y.T., Nguyen, P., Limqueco, E., Lopez, J., Thorossian, S., et al., 2016. Flow-dependent YAP/TAZ activities regulate endothelial phenotypes and atherosclerosis. Proceedings of the National Academy of Sciences of the United States of America 113:11525–11530.
[26] Colantuoni, A., Bertuglia, S., Intaglietta, M., 1984. Quantitation of rhythmic diameter changes in arterial microcirculation. American Journal of Physiology 246:H508–H517.
[27] Endrich, B., Asaishi, K., Gotz, A., Messmer, K., 1980. Technical report–a new chamber technique for microvascular studies in unanesthetized hamsters. Research in Experimental Medicine (Berl) 177:125–134.
[28] Kerger, H., Groth, G., Kalenka, A., Vajkoczy, P., Tsai, A.G., Intaglietta, M., 2003. pO(2) measurements by phosphorescence quenching: characteristics and applications of an automated system. Microvascular Research 65:32–38.
[29] Kunert, M.P., Liard, J.F., Abraham, D.J., Lombard, J.H., 1996. Low-affinity hemoglobin increases tissue PO2 and decreases arteriolar diameter and flow in the rat cremaster muscle. Microvascular Research 52:58–68.
[30] Gibson, Q.H., Gray, R.D., 1970. The reaction of inositol hexaphosphate with hemoglobin. Biochemical and Biophysical Research Communications 41:415–420.
[31] Intaglietta, M., Tompkins, W.R., 1973. Microvascular measurements by video image shearing and splitting. Microvascular Research 5:309–312.
[32] Lipowsky, H.H., Zweifach, B.W., 1978. Application of the "two-slit" photometric technique to the measurement of microvascular volumetric flow rates. Microvascular Research 15:93–101.
[33] Bornfeldt, K.E., Tabas, I., 2011. Insulin resistance, hyperglycemia, and atherosclerosis. Cell Metabolism 14:575–585.
[34] Hartvigsen, K., Binder, C.J., Hansen, L.F., Rafia, A., Juliano, J., Horkko, S., et al., 2007. A diet-induced hypercholesterolemic murine model to study atherogenesis without obesity and metabolic syndrome. Arteriosclerosis Thrombosis and Vascular Biology 27:878–885.
[35] Merat, S., Casanada, F., Sutphin, M., Palinski, W., Reaven, P.D., 1999. Western-type diets induce insulin resistance and hyperinsulinemia in LDL receptor-deficient mice but do not increase aortic atherosclerosis compared with normoinsulinemic mice in which similar plasma cholesterol levels are achieved by a fructose-rich diet. Arteriosclerosis Thrombosis and Vascular Biology 19:1223–1230.
[36] Attane, C., Peyot, M.L., Lussier, R., Zhang, D., Joly, E., Madiraju, S.R., et al., 2016. Differential Insulin Secretion of High-Fat Diet-Fed C57BL/6NN and C57BL/6NJ Mice: implications of Mixed Genetic Background in Metabolic Studies. PLoS One 11:e0159165.
[37] Zhao, Y., Ye, D., Wang, J., Calpe-Berdiel, L., Azzis, S.B., Van Berkel, T.J., et al., 2011. Stage-specific remodeling of atherosclerotic lesions upon cholesterol lowering in LDL receptor knockout mice. American Journal of Pathology 179:1522–1532.
[38] Tsimikas, S., Shortal, B.P., Witztum, J.L., Palinski, W., 2000. In vivo uptake of radiolabeled MDA2, an oxidation-specific monoclonal antibody, provides an accurate measure of atherosclerotic lesions rich in oxidized LDL and is highly sensitive to their regression. Arteriosclerosis Thrombosis and Vascular Biology 20:689–697.
[39] Cabrales, P., Tsai, A.G., Intaglietta, M., 2007. Perfluorocarbon in microcirculation during ischemia reperfusion. Journal of the American College of Surgeons 204:225–235.
[40] McNeill, E., Iqbal, A.J., Jones, D., Patel, J., Coutinho, P., Taylor, L., et al., 2017. Tracking monocyte recruitment and macrophage accumulation in

atherosclerotic plaque progression using a novel hCD68GFP/ApoE-/- reporter mouse-brief report. Arteriosclerosis Thrombosis and Vascular Biology 37: 258–263.

[41] Stoneman, V., Braganza, D., Figg, N., Mercer, J., Lang, R., Goddard, M., et al., 2007. Monocyte/macrophage suppression in CD11b diphtheria toxin receptor transgenic mice differentially affects atherogenesis and established plaques. Circulation Research 100:884–893.

[42] Swirski, F.K., Libby, P., Aikawa, E., Alcaide, P., Luscinskas, F.W., Weissleder, R., et al., 2007. Ly-6Chi monocytes dominate hypercholesterolemia-associated monocytosis and give rise to macrophages in atheromata. Journal of Clinical Investigation 117:195–205.

[43] Liu, H., Jiang, D., 2011. Fractalkine/CX3CR1 and atherosclerosis. Clinica Chimica Acta 412:1180–1186.

[44] Lesnik, P., Haskell, C.A., Charo, I.F., 2003. Decreased atherosclerosis in CX3CR1-/- mice reveals a role for fractalkine in atherogenesis. Journal of Clinical Investigation 111:333–340.

[45] Combadiere, C., Potteaux, S., Rodero, M., Simon, T., Pezard, A., Esposito, B., et al., 2008. Combined inhibition of CCL2, CX3CR1, and CCR5 abrogates Ly6C(hi) and Ly6C(lo) monocytosis and almost abolishes atherosclerosis in hypercholesterolemic mice. Circulation 117:1649–1657.

[46] Poupel, L., Boissonnas, A., Hermand, P., Dorgham, K., Guyon, E., Auvynet, C., et al., 2013. Pharmacological inhibition of the chemokine receptor, CX3CR1, reduces atherosclerosis in mice. Arteriosclerosis Thrombosis and Vascular Biology 33:2297–2305.

[47] White, G.E., McNeill, E., Channon, K.M., Greaves, D.R., 2014. Fractalkine promotes human monocyte survival via a reduction in oxidative stress. Arteriosclerosis Thrombosis and Vascular Biology 34:2554–2562.

[48] Robbins, C.S., Hilgendorf, I., Weber, G.F., Theurl, I., Iwamoto, Y., Figueiredo, J.L., et al., 2013. Local proliferation dominates lesional macrophage accumulation in atherosclerosis. Nature Medicine 19:1166–1172.

[49] Zhao, J., Nishimura, Y., Kimura, A., Ozawa, K., Kondo, T., Tanaka, T., et al., 2017. Chemokines protect vascular smooth muscle cells from cell death induced by cyclic mechanical stretch. Scientific Reports 7:16128.

[50] Landsman, L., Bar-On, L., Zernecke, A., Kim, K.W., Krauthgamer, R., Shagdarsuren, E., et al., 2009. CX3CR1 is required for monocyte homeostasis and atherogenesis by promoting cell survival. Blood 113:963–972.

[51] Hansson, G.K., Libby, P., Tabas, I., 2015. Inflammation and plaque vulnerability. Journal of Internal Medicine 278:483–493.

[52] Turner, R.C., Millns, H., Neil, H.A., Stratton, I.M., Manley, S.E., Matthews, D.R., et al., 1998. Risk factors for coronary artery disease in non-insulin dependent diabetes mellitus: United Kingdom Prospective Diabetes Study (UKPDS: 23). BMJ 316:823–828.

[53] Martin-Timon, I., Sevillano-Collantes, C., Segura-Galindo, A., Del Canizo-Gomez, F.J., 2014. Type 2 diabetes and cardiovascular disease: have all risk factors the same strength? World Journal of Diabetes 5:444–470.

[54] Schafer, A., Schulz, C., Eigenthaler, M., Fraccarollo, D., Kobsar, A., Gawaz, M., et al., 2004. Novel role of the membrane-bound chemokine fractalkine in platelet activation and adhesion. Blood 103:407–412.

[55] Meyer dos Santos, S., Klinkhardt, U., Scholich, K., Nelson, K., Monsefi, N., Deckmyn, H., et al., 2011. The CX3C chemokine fractalkine mediates platelet adhesion via the von Willebrand receptor glycoprotein Ib. Blood 117:4999–5008.

[56] Flierl, U., Bauersachs, J., Schafer, A., 2015. Modulation of platelet and monocyte function by the chemokine fractalkine (CX3 CL1) in cardiovascular disease. European Journal of Clinical Investigation 45:624–633.

